Structural Engineering and Mechanics, Vol. 14, No. 3 (2002) 331-343
DOI: http://dx.doi.org/10.12989/sem.2002.14.3.331

Ultimate behavior of long-span steel arch bridges

Jin Cheng† and Jian-Jing Jiang‡

Department of Civil Engineering, Tsinghua University, Beijing, 100084, China

Ru-Cheng Xiao‡ and Hai-Fan Xiang‡

Department of Bridge Engineering, Tongji University, Shanghai, 200092, China

(Received January 28, 2002, Accepted July 29, 2002)

Abstract. Because of the increasing span of arch bridges, ultimate capacity analysis recently becomes more focused both on design and construction. This paper investigates the static and ultimate behavior of a long-span steel arch bridge up to failure and evaluates the overall safety of the bridge. The example bridge is a long-span steel arch bridge with a 550 m-long central span under construction in Shanghai, China. This will be the longest central span of any arch bridge in the world. Ultimate behavior of the example bridge is investigated using three methods. Comparisons of the accuracy and reliability of the three methods are given. The effects of material nonlinearity of individual bridge element and distribution pattern of live load and initial lateral deflection of main arch ribs as well as yield stresses of material and changes of temperature on the ultimate load-carrying capacity of the bridge have been studied. The results show that the distribution pattern of live load and yield stresses of material have important effects on bridge behavior. The critical load analyses based on the linear buckling method and geometrically nonlinear buckling method considerably overestimate the load-carrying capacity of the bridge. The ultimate load-carrying capacity analysis and overall safety evaluation of a long-span steel arch bridge should be based on the geometrically and materially nonlinear buckling method. Finally, the in-plane failure mechanism of long-span steel arch bridges is explained by tracing the spread of plastic zones.

Key words: ultimate behavior; steel arch bridges; linear buckling; geometrically nonlinear buckling; geometrically and materially nonlinear buckling.

1. Introduction

Arch bridges have been very popular and widely used since ancient times. The reason for this is that arch bridges are aesthetically pleasing as well as economically feasible (Vlahinos *et al*. 1993). Nowadays, the maximum central span record of arch bridges is 518 m (New River Gorge Bridge, in U.S.A). With the completion of Lupu Bridge in Shanghai, China (550 m), the record will be broken. One of the main problems that have to be faced for such long spans is the evaluation of ultimate load-carrying capacity for arch bridges.

In the last decade, a number of studies have been performed to investigate the stability and load-

† Post-doctoral Fellow
‡ Professor

carrying capacity of arch bridges. These studies can be classified in three categories according to building material: reinforced concrete or masonry arch bridges (e.g., Ronca and Cohn 1979, McNeely *et al.* 1989, Clemente *et al.* 1995, Ng *et al*. 1999), concrete-filled steel tubular arch bridges (Yan and Han 1999), and steel arch bridges (e.g., Komatsu and Sakimoto 1977, Kuranishi and Yabuki 1984, Vlahinos *et al*. 1993, Nazmy 1997). To the writers' knowledge, no investigation on ultimate behavior of steel arch bridges has been published since Nazmy's work.

To analyze the ultimate capacity of arch bridges, the following methods are now available:

(1) the linear buckling method; (2) the geometrically nonlinear buckling method; (3) the geometrically and materially nonlinear buckling method. Because of its simplicity, the linear buckling method has been used in most ultimate capacity analyses of arch bridges (Kuranishi and Yabuki 1984, Vlahinos *et al.* 1993, Nazmy 1997). However, this method fails to take into consideration the effects of finite deformations as well as yielding of the material. These omissions could give dangerously misleading result in arch bridge with a compressive main member (Komatsu and Sakimoto 1977). Yan and Han (1999) studied the nonlinear instability of concrete-filled steel tubular arch bridge based on geometrically nonlinear buckling method. In their analysis, all geometric nonlinear sources were considered, but the material nonlinearity was not included. Ultimate behavior of reinforced concrete arch bridges has been investigated using a elastic-plastic hinge method (Ronca and Cohn 1979). But, since the plastic hinge method must assume full plasticity state of the cross section and can not treat the spread of plastic zones, it seems inadequate to apply the method directly to an instability analysis of structures having a compressive main member, whose plastic zones usually extend longitudinally and may not form an isolated plastic hinge (Komatsu and Sakimoto 1977). Komatsu and Sakimoto (1977) have proposed a method evaluating the rigidities of a partially yielded cross section, in which both the effects of finite deformations and spread of the plastic zones were considered. They have also studied the effect of other parameters (i.e., slenderness ratios, residual stresses, initial lateral deflections, loading directions and properties of the materials) on the ultimate strength and spatial elastic-plastic behavior of two-hinged parabolic arches. Because their parametric studies were based on two-hinged parabolic arches, their results may not be applied directly to the ultimate capacity analysis of long span steel arch bridges. Until now, however, the effect of other parameters (i.e., material nonlinear of individual bridge element, distribution pattern of live load, yield stresses of material and changes of temperature) on the ultimate behavior of long-span steel arch bridges has seldom been studied. In addition, the in-plane failure mechanism of long-span steel arch bridges has not been made clear so far.

In this paper, three methods to determine the ultimate carrying capacity of arch bridges are reviewed. Comparisons of the accuracy and reliability of the three methods are given. Attention is paid mainly to the following parameters, i.e., material nonlinear of individual bridge element, distribution pattern of live load, initial lateral deflection, yield stresses of material and changes of temperature. Their effects on the ultimate load-capacity of long-span steel bridges are examined. In addition to the parametric study, in-plane failure mechanism of long-span steel arch bridges is explained by tracing the spread of plastic zones.

2. Methods of analysis for ultimate loads

The aforementioned methods are briefly described in the following sections. A more detailed description may be obtained from Cheng (2002).

2.1 Linear buckling method

Assuming that the geometric stiffness, $[K_g]$, is proportional to the live load F, the linear incremental equilibrium equation may be expressed as:

$$([K_e] + \lambda[K_g]) \cdot \{\Delta u\} = \{\Delta F\} \tag{1}$$

in which $[K_e]$ represents the linear elastic stiffness matrix; $[K_g]$ represents the geometric elastic stiffness matrix; λ represents a scalar load intensity parameter; $\{\Delta u\}$ and $\{\Delta F\}$ represent the incremental displacement and force vectors, respectively.

The structure would buckle when the displacement increases without any increase in the load. At this time, $\{\Delta F\}$ becomes zero. Thus, Eq. (1) becomes:

$$([K_e] + \lambda[K_g]) \cdot \{\Delta u\} = \{0\} \tag{2}$$

Eq. (2) converts the buckling problem to the classical eigenvalue form that can be solved efficiently with any eigensolving method (i.e., the reduced, subspace, block Lanczos or QR damped methods).

2.2 Geometrically nonlinear buckling method

The geometrically nonlinear incremental equilibrium equations may be written as:

$$([K_e] + [K_g]) \cdot \{\Delta u\} = \{\Delta F\} \tag{3}$$

The solution of Eq. (3) is extensively reviewed in the literature. So will not discussed here. (See Torkamani *et al.* 1997, for further information). The detailed derivation of $[K_g]$ can be found in Yang and Kuo (1994). In this paper, to solve Eq. (3), an incremental-iterative method given by Teh and Clarke (1999) is used to obtain the load-deflection curve. The limit load of the structure is reached if one or more negative terms in the diagonal of the structure stiffness matrix are detected. To avoid too large or too small incremental load size, a load-displacement-constraint method is used. The basic idea of the method is to introduce a load multiplier that increases or decreases the intensity of the applied loads, so as to obtain fast convergence in each load step (Bathe 1996). A detailed description of the method may be obtained from Bathe (1996).

2.3 Geometrically and materially nonlinear buckling method

The geometrically and materially nonlinear incremental equilibrium equations can be written as:

$$([K_{ep}] + [K_g]) \cdot \{\Delta u\} = \{\Delta F\} \tag{4}$$

where $[K_{ep}]$ and $[K_g]$ are the elastic-plastic stiffness matrix and geometrical stiffness matrix, respectively. $[K_{ep}]$, is formulated by the von Mises yield criterion, the associated flow rule, and the hardening rule. The algorithm for forming $[K_{ep}]$ has been described by Pi and Trahair (1994), and is not repeated here. In this paper, an incremental-iterative method given by Teh and Clarke (1999) is

used to solve the Eq. (4). A local Newton-Raphson iteration procedure is used if the stress exceeds the material yield. This procedure has been described by Simo and Taylor (1985). To trace the limit load of the structure, a load-displacement-constraint method given by Bathe (1996) is used.

3. Modeling of the Lupu Bridge

3.1 Description of Lupu Bridge

The Lupu Bridge is the long-span welded steel half-through arch bridge under construction spanning the Huangpu River in Shanghai, China. It has a 550-m central span length, which will be the longest central span of any arch bridge in the world. The bridge span arrangements are (100 + 550 + 100) m. There are six traffic lanes. Rise-to-span ratio of the bridge is 1/5.5. Horizontal cables in the steel box girder are adopted to balance the horizontal force of the main arch rib. The tension of each horizontal cable is taken as 87900 KN, which is determined mainly by the horizontal force of the main arch rib. The elevation view of the bridge is shown in Fig. 1.

For the purposes of calculation, the cross-sectional shape is assumed to be a rectangular box section having the same cross-sectional properties as the actual cross sections of the bridge. The elevation view of the arch rib of the bridge is shown in Fig. 2. The cross-sectional properties of the arch rib are listed in Table 1. Table 2 shows the cross-sectional properties of steel box girder. The material data for the analyses are listed in Table 3.

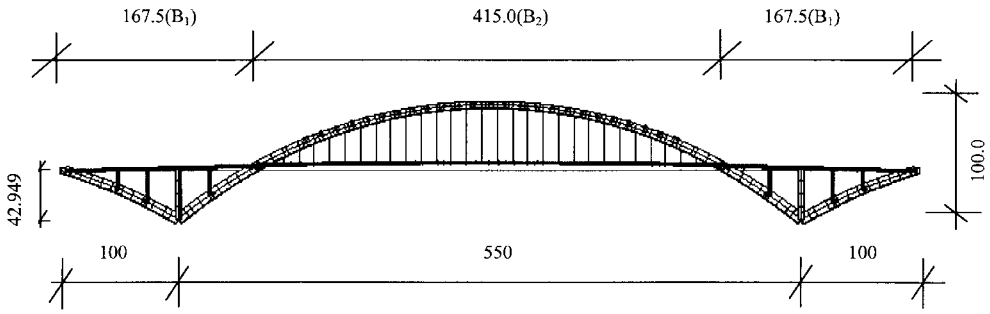

Fig. 1 Elevation of Lupu Bridge (Unit: m)

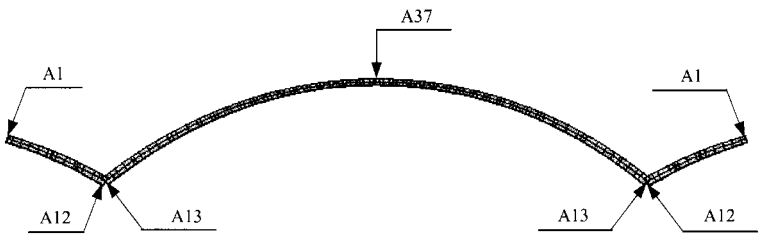

Fig. 2 Elevation of arch rib of Lupu Bridge

Table 1 Cross-sectional properties data of arch rib

Section number of arch rib	Area (m^2)	In-plane moment of inertia (m^4)	Out-of-plane moment of inertia (m^4)	Torsional moment of inertia (m^4)
A1	0.82005	5.6257	1.8978	4.4293
A2	0.82446	5.8448	1.9250	4.5250
A3	0.83571	6.1983	2.0064	4.7366
A4	0.83752	6.5855	2.0454	4.8909
A5	0.84752	7.0325	2.1035	5.0857
A6	0.85822	7.4877	2.1659	5.2869
A7	0.87441	7.9761	2.2450	5.5216
A8	0.86979	8.3088	2.2632	5.6171
A9	0.88291	8.7623	2.3343	5.8276
A10	0.88743	9.2121	2.3739	5.9809
A11	0.89287	9.5754	2.4174	6.1202
A12	0.89432	9.7044	2.4307	6.1623
A13	0.99933	10.964	2.6287	6.7516
A14	0.99866	10.860	2.6194	6.7186
A15	0.99437	10.562	2.5888	6.6133
A16	0.98886	10.205	2.5492	6.4805
A17	0.98241	9.8406	2.5073	6.3413
A18	0.97636	9.4935	2.4632	6.2003
A19	0.97048	9.1596	2.4237	6.0693
A20	1.5546	14.742	3.5462	9.0892
A21	1.5462	14.134	3.4992	8.8774
A22	1.5375	13.568	3.4165	8.6649
A23	0.86813	6.9717	2.2842	5.3692
A24	0.87177	6.6416	2.2160	5.1776
A25	0.86310	6.2758	2.1593	4.9961
A26	0.85048	5.9192	2.0913	4.7989
A27	0.84936	5.6341	2.0597	4.6712
A28	0.84187	5.3989	1.9964	4.5178
A29	0.83997	5.1521	1.9645	4.3985
A30	0.83330	4.9105	1.9201	4.2620
A31	0.82858	4.6980	1.8829	4.1430
A32	0.82114	4.5008	1.8423	4.0242
A33	0.81920	4.3413	1.8140	3.9317
A34	0.81265	4.1936	1.7779	3.8338
A35	0.80804	4.0811	1.7531	3.7626
A36	0.80520	4.0225	1.7471	3.7323
A37	0.80469	3.9565	1.7331	3.6826

Table 2 Cross-sectional properties data of steel girder

Section number of steel girder	Area (m^2)	In-plane moment of inertia (m^4)	Out-of-plane moment of inertia (m^4)	Torsional moment of inertia (m^4)
B1	1.7751	2.8349	290.62	10.05
B2	1.1422	1.3950	174.72	5.1374

Table 3 Material data of Lupu Bridge

Material	E (GPa)	α	ν	σ_y (MPa)	ρ (kg/m^3)
Steel	210.0	0.000012	0.30	345.0	7850.0
Hangers and Cables	200.0	0.000012	0.30	____	8400.0

Note: E: Elastic modulus; α: Coefficients of thermal expansion; ν: Poisson's ratio; σ_y: Yield stress of material; ρ: Weight per unit volume of material

3.2 Assumptions

The following assumptions were made:

· There is no effect on the material properties due to temperature variations.
· No local buckling is considered.
· In the elastic-plastic ultimate capacity analysis, the elastic-plastic behavior of the steel girder and arch ribs is only considered. In other words, hangers, arch bracing, spandrel column and horizontal cable in the steel box girder are assumed to remain elastic throughout.
· Initial live load, q_0, is taken as 40 KN/m. Live load factor, n, can be written by

$$n = \frac{q_l}{q_0} \tag{5}$$

where q_l is the applied live load. In this paper, because that dead loads of the example bridge change due to the bridge cross-section variation, the overall safety factor of the bridge is determined by the maximum live load factor.

3.3 Finite-element model of Lupu Bridge

A detailed finite element model of the Lupu Bridge was developed in the present study (Fig. 3). Various parts of the Lupu Bridge are illustrated in Fig. 3. For FEM modeling, the bridge deck is represented by a single beam and the cross-section properties of the bridge deck are assigned to the beam as equivalent properties. The bridge deck, arch ribs, arch bracing and spandrel column are modeled by 3D-beam element. The hangers and horizontal cable in the steel box girder are modeled by 3D-truss element. The finite element model contains 741 elements, 669 nodes.

The actual boundary conditions are as follows: the joint between the main girder and side arch rib is a movable hinge (roller) support as shown in Fig. 3. The main arch ribs are fixed at the abutments.

4. Ultimate behavior under live loads

This section examines three methods of analyzing ultimate load-capacity of long-span arch bridges under live load uniformly distributed in all spans and gives the comparisons of the accuracy and reliability of the three methods. The live loads are applied starting from the deformed configuration of the bridge due to dead loads. The results of analysis for the live load factor using the three methods described above are presented in Table 4. Load-displacement curves of arch rib

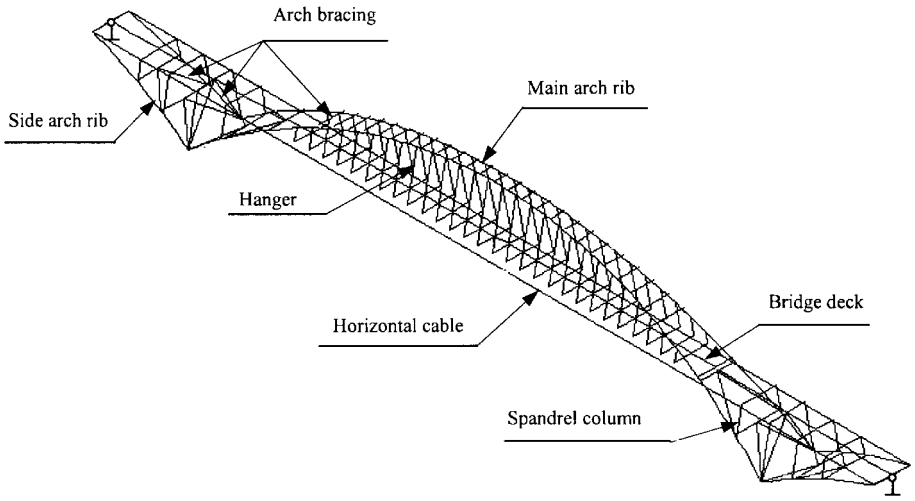

Fig. 3 3D Finite element model of Lupu Bridge

Table 4 Comparison of maximum live load factor for various methods

Method	Linear Buckling	Geometrically Nonlinear Buckling	Geometrically and Materially Nonlinear Buckling
n	48	41.25	17.638

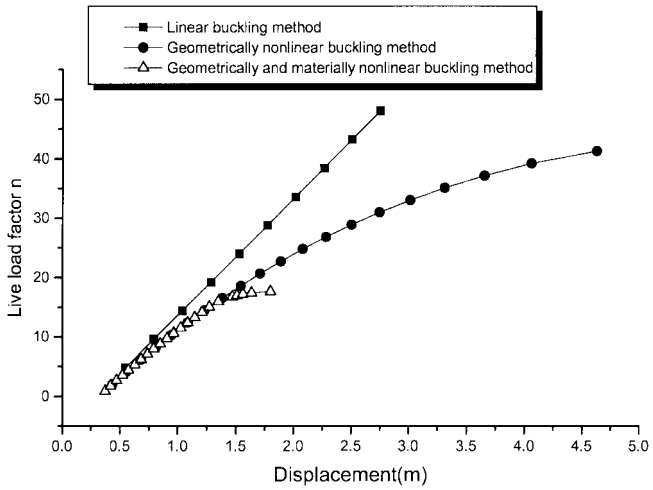

Fig. 4 Load-deflection (vertical) curve at midpoint of main arch rib for various methods

obtained from the three methods are shown in Fig. 4. As can be seen in the Figure, the ultimate capacity of the bridge predicted by the geometrically and materially nonlinear buckling method is significantly less than the prediction of the linear buckling method and geometrically nonlinear

buckling method. The maximum live load factor of 17.638 obtained from the geometrically and materially nonlinear buckling method is 57.2% lower than that of 41.25 obtained from geometrically nonlinear buckling method and 63.3% lower than that of 48.0 obtained from linear buckling method.

5. Parametric study

A parametric study of the Lupu Bridge was conducted to investigate how material nonlinearity of individual bridge element, distribution pattern of live load, initial lateral deflection of main arch ribs and yield stresses of material and changes of temperature affect the ultimate capacity of long-span arch bridges. In all but some of Sec.5.3 cases, the geometrically and materially nonlinear buckling method is used.

5.1 Effect of material nonlinearity of individual bridge element

To investigate the material nonlinearity effects of individual bridge element, three cases are considered. Case I: Only the steel girder is considered elastic-plasticity; all other bridge elements are assumed to be elastic. Case II: Only steel arch ribs are considered elastic-plasticity; all other bridge elements are assumed to be elastic. Case III: Both steel girder and the arch ribs are considered elastic-plasticity; all the other bridge elements are assumed to be elastic. The maximum live load factors in these three cases are summarized in Table 5. As can be seen in this Table, the maximum live load factor in Case II is the same as that of Case III, which implies that the material nonlinearity of arch ribs has significant effect on the ultimate capacity. However, the material nonlinearity of steel girder has no effect on the ultimate capacity. Therefore, the material nonlinearity of steel girder may not be considered in the ultimate behavior analysis of long-span arch bridges.

5.2 Effect of yield stresses of material

In addition to the actual yield stress of steel (σ_y = 345 MPa), two other kinds of yield stress of steel (σ_y = 382 MPa and σ_y = 420 MPa) are used in the following ultimate capacity analysis. The maximum live load factors for various yield stresses of steel are listed in Table 6. Load-displacement (vertical) curves of arch ribs for various yield stresses of steel are shown in Fig. 5.

Table 5 Comparison of maximum live load factor for various cases

Case	Case I	Case II	Case III
n	41.25	17.638	17.638

Table 6 Maximum live load factors for various yield stresses of steel

Yield Stress of Steel (MPa)	345	382	420
n	17.638	19.625	21.625

The figure indicates that the ultimate capacity increases as the yield stress of material (steel) increases. In addition, the figure also indicates that the initiation of yielding will occur earlier as yield stress of material (steel) decreases.

5.3 Effect of distribution pattern of live load

This section comprises two analytical steps. First, the effect of live loads on the geometric nonlinear behavior of a long-span steel arch bridge was investigated using the geometrically nonlinear buckling method. Linear analysis results are also given for the comparison. In the second analysis step, the effect of live loads on the ultimate behavior of a long-span steel arch bridge is investigated. The geometrically and materially nonlinear buckling method is used in the second analysis step. Two live load cases are considered in the two analysis steps. Live load case I is the live load uniformly distributed in all spans. Live load case II is the live load uniformly distributed only in the left half of central span. Figs. 6 and 7 give the load-displacement curves under live load cases I and II, respectively. Fig. 8 gives the comparison of the ultimate behavior under live load cases I and II. It is seen from Figs. 6 and 7 that geometric nonlinearity of the bridge has a larger effect on the static behavior under live load case II than that under live load case I. As can be seen in Fig. 8, the ultimate loads under live load case II are lower than live load case I, so that live load case II (uniformly distributed only in the left half of central span) is more harmful to the bridge.

5.4 Effect of initial lateral deflection of main arch ribs

To investigate the effect of initial lateral deflection of main arch ribs on the ultimate capacity, the main arch ribs are assumed to have initial lateral deflection ω. The initial lateral deflection, ω, can be expressed as:

$$\omega = \omega_0 \cdot \sin\frac{\pi x}{l} \tag{6}$$

where ω_0 is the initial lateral deflection at the midpoint of the main arch ribs; l is the length of

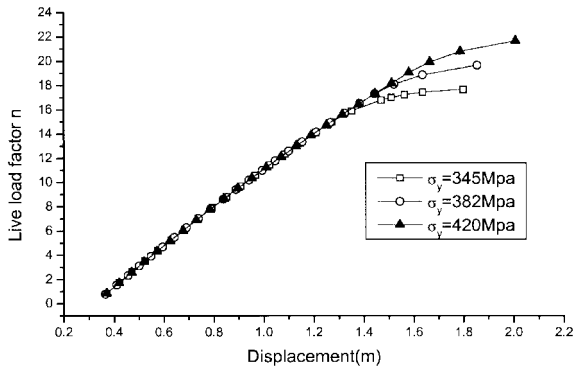

Fig. 5 Load-deflection (vertical) curve at midpoint of main arch rib for various yield stresses of material

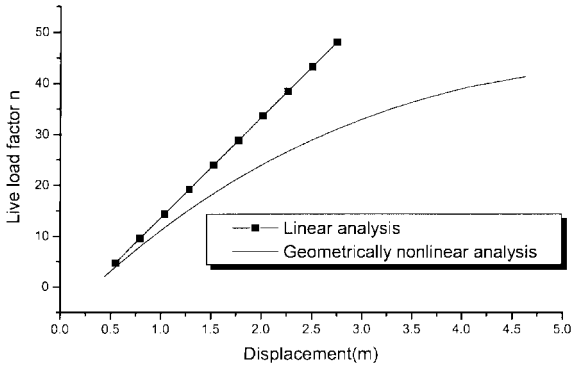

Fig. 6 Load-deflection (vertical) curve at midpoint of main arch rib under live load Case I

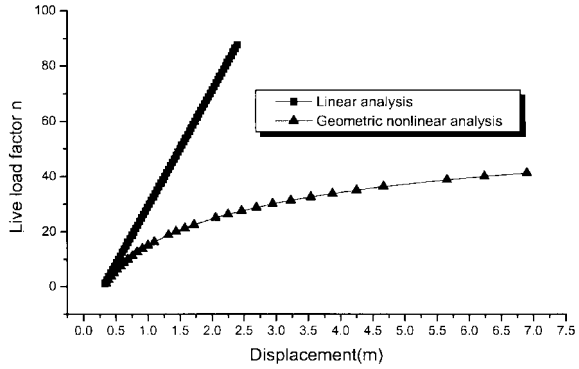

Fig. 7 Load-deflection (vertical) curve at midpoint of main arch rib under live load Case II

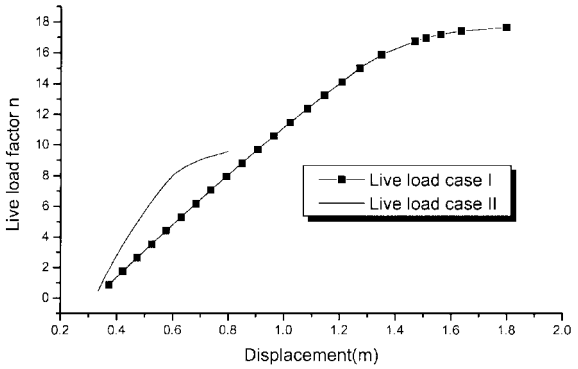

Fig. 8 Comparison of the ultimate behavior (vertical) at midpoint of main arch rib under live load Case I and II

Table 7 Comparison of maximum live load factor for various initial lateral deflection of main arch ribs

ω_0	l/5000	l/1000	l/500
n	17.625	17.56	17.50

central span. In this section, ω_0 is given values l/5000, l/1000, l/500, respectively. The results are summarized in Table 7. This Table shows that initial lateral deflection of main arch ribs has a minor effect on the in-plane ultimate capacity of long-span steel arch bridges.

5.5 Effect of changes of temperature

In this section, three cases are considered in the following ultimate capacity analysis. Case I: dead loads + elevated temperature of 60^o + live loads uniformly distributed in all spans; Case II: dead loads + live loads uniformly distributed in all spans; Case III: dead loads + lowered temperature of 15^o + live loads uniformly distributed in all spans. Fig. 9 shows the load-deflection curves due to the change of temperature. It is seen from this figure that the change of temperature has a minor effect on the ultimate capacity of steel arch bridge. Generally speaking, the ultimate capacity of bridge increases as the temperature elevates and decreases as the temperature lowers. This is due to the axial force in the arch ribs is changed when the temperature of bridge is changed.

6. In-plane failure mechanism of steel arch bridges

Until now the in-plane instability mechanism of steel arch bridges has seldom been studied. In this section, the in-plane instability mechanism of steel arch bridges is explained by tracing the plastic zone spread of the Lupu Bridge as mentioned above. In the following figures, the symbol "▪" denotes the plastic zones due to compression. To display the deformation of structure distinctly,

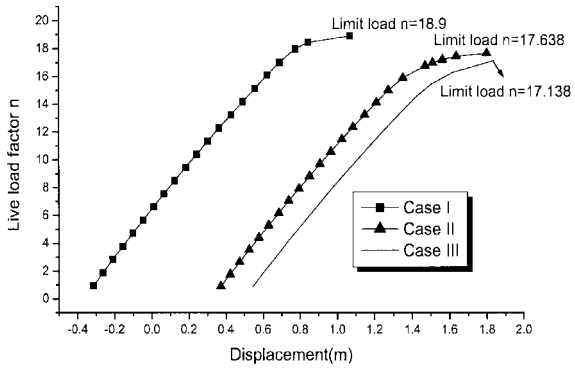

Fig. 9 Load-deflection (vertical) curve at midpoint of main arch rib for various Cases

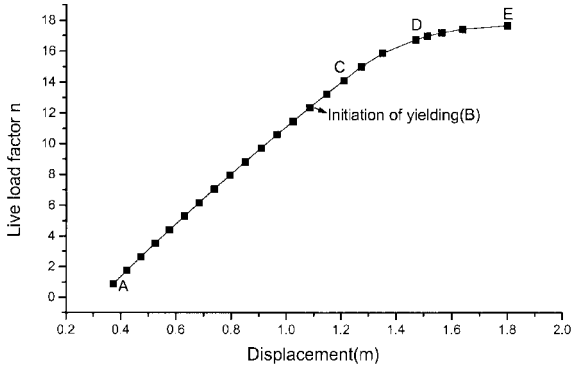

Fig. 10 Load-deflection (vertical) curve at midpoint of main arch rib under live load Case I

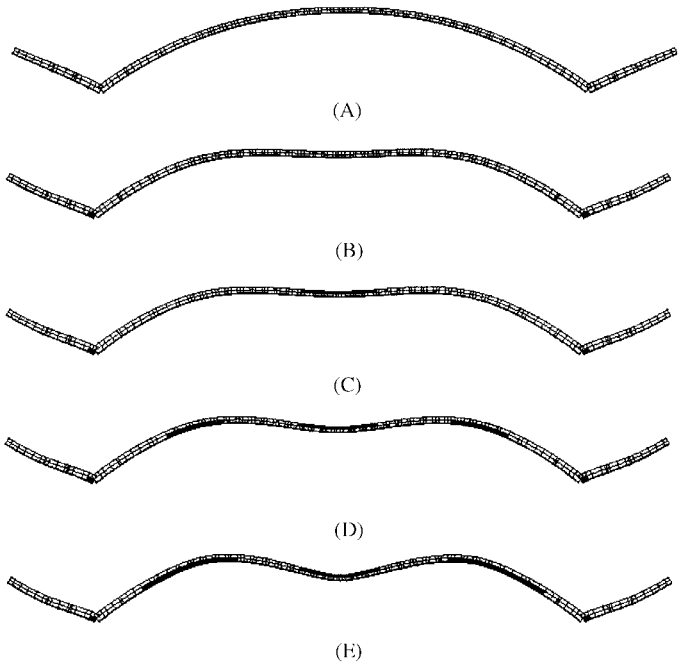

Fig. 11 Deformed shapes of arch rib under live load Case I: (A) deformed shape of arch rib (n = 0.8819); (B) deformed shape of arch rib (n = 12.346); (C) deformed shape of arch rib (n = 14.11); (D) deformed shape of arch rib (n = 16.756); (E) deformed shape of arch rib (n = 17.638)

displacements in the figures are magnified by 30 times. The one to one correspondence between the deformation of arch ribs and live load factor are labeled as A, B, C, D and E in Figs. 10 and 11. Fig. 10 shows load-deflection curve of arch ribs under live load uniformly distributed in all spans, which is obtained by using geometrically and materially nonlinear buckling method. Deformed shapes of arch ribs at various live load factors are shown in Fig. 11. From Figs. 10 and 11, it can

been seen that the vertical displacement of midpoint of central span for arch ribs is small; the whole structure is in the range of elasticity at the point "A". With increasing load, the vertical displacement of midpoint of central span for arch ribs also increases. At the point "B"(initiation of yield), although the flexural compression stress at the bottom of arch base section is equal to the yield stress of material, the structure is not unstable. But, the stiffness of structure is lowered by the yield at the bottom of arch rib section. Stress redistribution begins upon initiation of yield. At the point "C", the flexural compression stress at the top of arch crown section is equal to the yield stress of material at the live load factor of 14.11. At this time, the top of arch crown section begins to yield, too. The plastic zones at the arch crown spread rapidly as the live loads increase. At the point "D", the capacity of structure decreases quickly when the flexural compression stress at the bottom of 1/4 point of central span is equal to the yield stress of material. The failure of arch ribs takes place at the point "E". The overall failure of the arch bridge is triggered by the collapse of arch ribs. The system's limit of resistance is indicated by the first negative diagonal element in the stiffness matrix when the bridge reaches its maximum capacity at the live load factor of 17.638.

7. Conclusions

Based on a comprehensive ultimate behavior analysis of a long-span steel arch bridge, it can be concluded that:

(1) The critical (buckling) load analyses of steel arch bridges based on the linear buckling method and geometrically nonlinear buckling method considerably overestimate the load-carrying capacity so that they give unsafe results. The actual ultimate load-carrying capacity should be evaluated based on geometrically and materially nonlinear buckling method. The ultimate load-carrying capacity of long-span steel arch bridges is mainly controlled by the material nonlinearity.

(2) Between the nonlinear material behavior of the girder and the arch ribs, the ultimate load carrying of the steel arch bridge primarily depends on the failure of the arch ribs.

(3) Yield stress of material is an important parameter that influences the ultimate capacity of long-span steel arch bridges under both live and dead load. As the yield stress of material increases, the bridge limit load and its resistance to vertical loads increase.

(4) The distribution pattern of live load is another important parameter that affects ultimate capacity of long-span steel arch bridges under dead and live loads. With regard to live loads, in the most cases, live load case II (uniformly distributed only in the left half of central span) is more harmful to the long-span steel arch bridge.

(5) Changes of temperature and initial lateral deflection of main arch ribs have minor effects on in-plane ultimate capacity of long-span steel arch bridges.

Acknowledgements

The writers would like to thank to the National Nature Science Foundation of China under grant number 59895410 for their financial support. The valuable comments of the anonymous reviewers of the paper are also acknowledged.

References

Bathe, K.J. (1996), *Finite Element Procedures*, Prentice-Hall, Englewood Cliffs, N.J.
Cheng, J. (2002), "Study on some issues in long-span bridges", Post-doctoral Research Report (in Chinese), Tsinghua University.
Kuranishi, S. and Yabuki, T. (1984), "Lateral load effect on steel arch bridge design", *J. Struct. Eng.*, **110**(9), September, 2263-2274.
Lip, H. Teh and Murray, J. Clarke (1999), "Plastic-zone analysis of 3D steel frames using beam elements", *J. Struct. Eng.*, **125**(11), November, 1328-1337.
McNeely, D.K. Archer, G.C. and Smith, K.N. (1989), "Structural analysis of old stone arch bridges", *Canadian Journal of Civil Engineering*, **16**(6), Dec, 789-797.
Morteza, A.M. Torkamani, Mustafa, Sonmez and Jianhua, Cao (1997), "Second-order elastic plane-frame analysis using finite-element method", *J. Struct. Eng.*, **123**(9), September, 1225-1235.
Nazmy, A.S. (1997), "Stability and load-carrying capacity of three-dimensional long-span steel arch bridges", *Comput. Struct.*, **65**(6), 857-868.
Ng, K.H., Fairfield, C.A. and Sibbald, A. (1999), "Finite-element analysis of masonry arch bridges", *Proceedings of the Institution of Civil Engineers, Structures and Buildings*, **134**(2), 119-127.
Paola, Ronca and Cohn, M.Z. (1979), "Limit analysis of reinforced concrete arch bridges", *J. Struct. Div.*, ASCE, **105**(ST2), February, 313-326
Paolo, Clemente, Antonio, Occhiuzzi and Aldo, Raithel (1995), "Limit behavior of stone arch bridges", *J. Struct. Eng.*, **121**(7), July, 1045-1050.
Sadao, Komatsu and Tatsuro, Sakimoto (1977), "Ultimate load carrying capacity of steel arches", *J. Struct. Div.*, ASCE, **103**(ST12), December, 2323-2336.
Simo, J.C. and Tayor, R.L. (1985), "Consistent tangent operators for rate independent elasticoplasticity", *Comp. Meth. Appl. Mech. Engrg.*, **48**, 101-108.
Vlahino, A.S., Ermpoulos, J.Ch. and Wang, Y.C. (1993), "Buckling analysis of steel arch bridges", *J. Construct. Steel Research*, **26**, 59-71.
Yan, Q.S. and Han, D.J. (1999), "Nonlinear stability of the Jiefang concrete-filled steel tube tie-bar arch bridges", *Journal of South China University of Technology*, **27**(11), 98-103 (in Chinese).
Yong, Lin Pi and Trahair, N.S. (1994), "Nonlinear inelastic analysis of steel beam-columns I: Theory", *J. Struct. Eng.*, **120**(7), July, 2041-2061.